

Design of a Fe₄S₄ cluster into the core of a de novo four-helix bundle

Joshua A. Mancini 101,2
Douglas H. Pike2
Alexei M. Tyryshkin1
Liti Haramaty1
Michael S. Wang3
Saroj Poudel1,2
Michael Hecht 103
Vikas Nanda 102*

¹Environmental Biophysics and Molecular Ecology Program, Department of Marine and Coastal Sciences, Rutgers University, New Brunswick, NJ, USA

²Department of Biochemistry and Molecular Biology, Robert Wood Johnson Medical School and the Center for Advanced Biotechnology and Medicine, Rutgers University, Piscataway, NJ, USA

Abstract

We explore the capacity of the *de novo* protein, S824, to incorporate a multinuclear iron–sulfur cluster within the core of a single-chain four-helix bundle. This topology has a high intrinsic designability because sequences are constrained largely by the pattern of hydrophobic and hydrophilic amino acids, thereby allowing for the extensive substitution of individual side chains. Libraries of novel proteins based on these constraints have surprising functional potential and have been shown to complement the deletion of essential genes in *E. coli*. Our structure-based design of four first-shell cysteine ligands, one per helix, in S824 resulted in successful

incorporation of a cubane Fe₄S₄ cluster into the protein core. A number of challenges were encountered during the design and characterization process, including nonspecific metal-induced aggregation and the presence of competing metal-cluster stoichiometries. The introduction of buried iron–sulfur clusters into the helical bundle is an initial step toward converting libraries of designed structures into functional *de novo* proteins with catalytic or electron-transfer functionalities. © 2020 International Union of Biochemistry and Molecular Biology, Inc. Volume 67, Number 4, Pages 574–585, 2020

Keywords: de novo protein, iron–sulfur cluster, combinatorial library, protein design, electron transfer, oxidoreductase

Abbreviations: CD, circular dichroism; E. coli, Escherichia coli; EPR, electron paramagnetic resonance; Fe–S, Iron–sulfur; MD, molecular dynamics; NHE, normal hydrogen electrode; NMR, nuclear magnetic resonance; UV–vis, ultraviolet–visible.

*Address for correspondence: Vikas Nanda, PhD, Center for Advanced Biotechnology and Medicine, 679 Hoes Lane West, Piscataway, NJ 08854-8021, USA. Tel: +1 848 445 9810; email: nandavi@cabm.rutgers.edu Joshua A. Mancini and Douglas H. Pike contributed equally.

Additional supporting information may be found online in the Supporting Information section at the end of the article.

Received 9 July 2020; accepted 6 August 2020

DOI: 10.1002/bab.2003

Published online 21 August 2020 in Wiley Online Library (wileyonlinelibrary.com)

1. Introduction

The α -helical bundle, a topology comprising several α -helices twisted around a central axis, is abundant among natural proteins [1,2]. The bundle is also a fertile scaffold for designing novel proteins [3]. Four-helix bundles have a high intrinsic "designability" because a large set of potential sequences can assume nearly identical helical folds [4,5]. Thus, repetition of a seven-residue sequence pattern with the first and fourth positions specified as hydrophobic and the remaining positions specified as hydrophilic is often sufficient to produce folded, stable α -helical bundles [6]. Because the pattern of polar and nonpolar residues plays such a dominant role in dictating the structure of the helical bundle, the exact identities of the side chains can be varied. This facilitates the construction of vast libraries of novel sequences in which the binary pattern

³Department of Chemistry, Princeton University, Princeton, NJ, USA

of polar and nonpolar residues is held constant, while the exact sequence is varied combinatorially [7]. Several such binary patterned libraries have been designed. However, it is noteworthy that they were designed for structure, but were not explicitly designed for any particular activities or functions. Nonetheless, proteins isolated from binary pattern libraries have been shown to provide life-sustaining functions in *E. coli* [8–12]. This nascent functionality imbedded in these proteins can be enhanced through laboratory-based evolution [13] and/or computational design to produce functionally useful cofactors.

Metals and metal-containing prosthetic groups provide both structural stability and functional reactivity to proteins. The earliest proteins in metabolism were likely redox metalloprotein catalysts [14]. Natural metalloproteins that evolved from these early ancestors can also be further modified in the laboratory to generate new metalloproteins, which take advantage of metals' range of oxidation states, electron transfer capacities, and Lewis acidities to produce new biocatalysts. For example, natural cytochrome P450s, a family of heme proteins that catalyze a broad spectrum of chemical transformations, have been used as starting points to produce collections of mutants that can be optimized through laboratory evolution to produce industrial catalysts [15]. Another prominent example is the recent demonstration that a redox potential of a metal cofactor in the native protein azurin can be systematically tuned, by point mutations and metal cofactor exchange, covering the entire physiological range from -1 to +1 V vs normal hydrogen electrode (NHE) [16]. In addition to using natural proteins as starting materials for laboratory evolution, it is also possible to develop entirely novel proteins—such as helical bundles incorporating c-type hemes—toward a wide range of reactions of industrial and pharmaceutical importance [17].

Rational protein design has produced a number of synthetic metalloenzymes that incorporate metals within the core of helical bundles [18–23]. The residues surrounding the metal can then be modified to tune the reduction potential and reactivity of the resulting active sites [24–29] or to create substrate channels that modulate specificity [30]. Combinatorial libraries have also produced four-helix bundles that bind metals. A recent study showed that proteins from binary patterned libraries bind a range of metal ions, largely through coordination by surface-exposed imidazole and carboxylate side chains [31]. Additionally, a significant number of binary patterned helical bundles were shown to bind heme through histidine and methionine coordination [32–34].

The burial of metal ions and the polar residues that bind these metals comes with a cost to the stability of the folded state. In particular, for binary patterned libraries, incorporating metals or metal cofactors would require core-facing side chains that violate the polar/nonpolar pattern that specifies a fully hydrophobic core. Nonetheless, the observed metal binding and functional potential of binary patterned libraries suggests that many of these bundles are stable enough to tolerate the introduction of destabilizing metal sites into their cores. To

Research Highlights

- (1) *De novo* proteins are designed based on physical principles of protein structure.
- (2) A four-iron four-sulfur metal cluster binding site was successfully introduced into a *de novo* protein.
- (3) The *de novo* metalloprotein is redox active and can be a starting point for functional oxidoreductase designs.

probe this tolerance, we chose one of the most stable binary patterned proteins, S824 [35], as a structural scaffold for the design of a buried site for an iron–sulfur cluster.

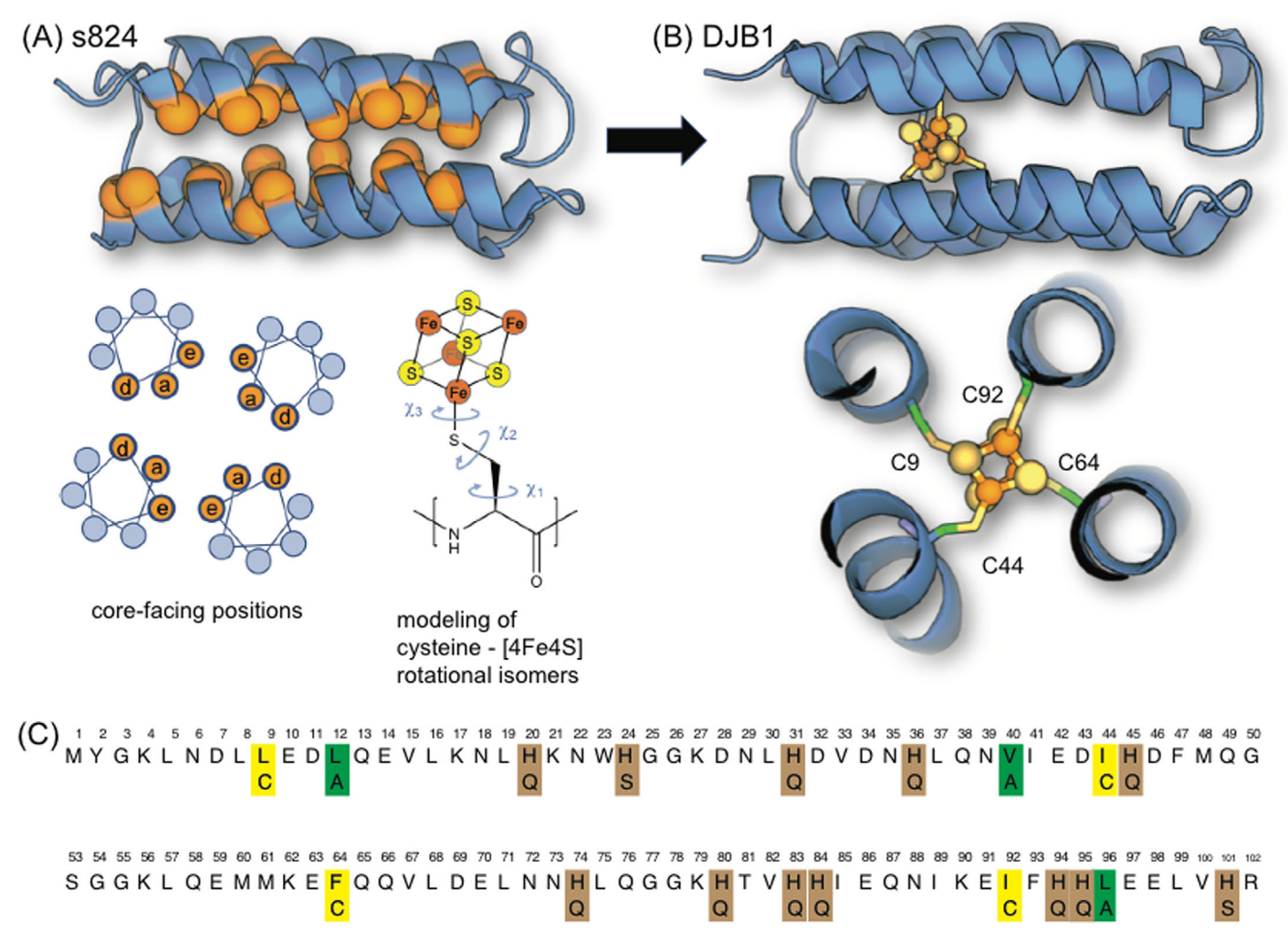
Iron–sulfur (Fe–S) clusters are common metal cofactors, essential to all living organisms. Proteins containing Fe–S clusters are ubiquitous in all three domains of life and are responsible for transferring electrons and catalyzing redox reactions that sustain life [36]. These reactions include photosynthesis, nitrogen fixation, hydrogen oxidation, and carbon fixation [37–41]. Fe–S clusters in natural proteins are predominantly found in three structural forms, Fe₂S₂, Fe₃S₄, and Fe₄S₄, with the latter being most widespread [42,43]. The broad involvement of Fe–S clusters in essential biochemical functions is likely due to the abundance of iron on earth, and the ability of iron to switch between different oxidation states (e.g., +2 and +3). The diverse forms of Fe–S clusters cover a wide range of redox potentials ranging from -700 to +500 mV (vs NHE), readily tunable by the protein environment surrounding the cluster [44].

Redox-active Fe-S clusters can serve as new features to build tunable catalytic or electron-transfer functions into libraries of proteins that were initially designed solely for the structure. In the current study, a Fe₄S₄ cluster is designed into the core of S824, a stable and well-characterized member of a binary pattered library of four-helix bundles [35,45,46]. The resulting protein—DJB1—is related to previous designs [36,37], where the metal coordination environment was designed to match the preexisting geometry of the protein scaffold. However, DJB1 differs from both previous designs [47-52] and all known natural iron-sulfur proteins in that the four metal-binding cysteines are well separated in the primary sequence, with each located on a different α -helix. The four ligand positions were chosen by computationally probing all residue combinations and identifying energetically and geometrically feasible solutions [53]. The design, experimental characterization, and optimization protocol are described and serve as a guide for future designs of libraries of novel metalloproteins.

2. Methods

2.1. Design of a Fe₄S₄-binding site into S824

The published NMR structure of S824 (PDB: 1p68, first model) [35] was used as a starting template to design the new



Design of a Fe_4S_4 cluster-binding site into a de novo four-helix bundle: (A) The NMR structure of binary patterned de novo protein S824 (PDB: 1p68) [35] was used as a starting structure. All side chains were removed to produce a backbone template for designing a Fe_4S_4 -binding site. Each residue in the structure was then mutated to a cysteine ligated to a Fe_4S_4 (bottom right in panel A) to determine which core sites had the fewest clashes with the S824 backbone. Orange-colored positions were found suitable for coordinating the Fe_4S_4 cofactor. (B) F64C was chosen as the optimal mutation for addition of a core Fe_4S_4 cluster. Three remaining cysteine positions were chosen based on the closest proximity to three other irons of the Fe_4S_4 at this site. (C) The amino acid sequence of the parent protein S824, where yellow point mutations are cysteines for Fe_4S_4 coordination, green are alanine mutations required to minimize unfavorable van der Waals contacts, and brown are histidine to glutamine/serine mutations to eliminate extraneous Fe^{2+}/Fe^{3+} coordination and to minimize interbundle aggregation. The S824 sequence with all the indicated mutations is named a DJB1-noHis.

bundle variants. For each position in the four-helix bundle, Lennard-Jones potentials for van der Waals contacts, as parameterized in AMBER [54], were calculated between the Fe₄S₄-decorated cysteine residue (low right in Fig. 1A) and all backbone atoms of S824. Three rotational degrees of freedom (χ_1 , χ_2 , χ_3) were sampled on the Fe₄S₄-cysteine residue to determine its optimum packing arrangement inside the bundle core, while maintaining a native-like coordination geometry between the cysteine and Fe₄S₄. The lowest van der Waals energy was established for the mutation F64C within the S824 core (Fig. 1B). Three other cysteines were then added to S824 based on their beta-carbon proximity to the

three remaining irons of the Fe_4S_4 cluster at this low-energy configuration. The resulting S824 variant with a full Fe_4S_4 coordination was then side chain optimized using the Dunbrack rotamer library [55], and any remaining side chain clashes with the cluster were mutated to alanine (Fig. 1C), resulting in our first Fe_4S_4 coordinating variant, DJB1. Additional mutations replacing histidine with glutamine in a helical conformation or serine in a loop were done manually using the mutation function in pyMol [56]. The apo DJB1 model was prepared by removing the cluster and protonating the cysteines which were originally coordinated to the Fe_4S_4 cluster in the holo-protein.

F1G.1

2.2. Molecular dynamics simulations

The NMR-derived structure of S824 (PDB: 1p68, first model) [35] was used as a starting configuration for all molecular dynamics (MD) simulations, including the parent protein, S824, and its DJB1-noHis modifications. The initial position for an Fe₄S₄ cluster in DJB1-noHis was defined by modeling the lowest energy cysteine-cluster coordinated position using protCAD [57,58]. Additional mutations as required were performed manually using PyMol [56]. DJB1-noHis/apo used the same model as DJB1-noHis/Fe₄S₄ where the cluster was removed, and all cysteines were protonated. AMBER explicit MD simulations were performed using the ff14SB force field [59] and the SF4 force-field modifications previously reported [60], with an atomic distance cutoff of 8 Å. Models were solvated in TIP3P water and minimized in steepest descent, followed by conjugate gradient minimization. Periodic boundaries were set under constant volume, and the system was thermalized from 0 to 300 K using Langevin dynamics and a collision frequency of 3 ps⁻¹. MD simulations were run for 500 nSec at 300 K. Calculations were performed with a 2-fs time step, and rootmean square deviation (RMSD) analysis was done every 10,000 steps using the visual molecular dynamics software [61].

2.3. Plasmids for protein expression

The expression plasmids, p3GLAR [8], were linearized using the following primers:

Forward: CTAACTTAATTAGCTGAGCTTGGAC

Reverse: TGTAATTTCTCCTCTTTAATGAATTCTGT

DNA constructs were ordered as gene fragments from IDT (Integrated DNA Technologies, San Jose, CA, USA) with overhangs on the 5' and 3' ends, homologous to the 5' and 3' ends of the linearized p3GLAR backbone. HiFi assembly master mix from New England Biolabs (Ipswich, MA, USA) was used to assemble gene fragments into plasmids.

2.4. Protein expression

All proteins were expressed from the p3GLAR plasmid under selection for chloramphenicol resistance [8]. The expression plasmids were transformed into $E.\ coli$ strain BL21DE3. Initially, cells were grown overnight at 37 °C from a single colony inoculated in 50 mL of Luria-Bertani (LB) media. The next day, the 50-mL cultures were diluted into 500 mL and grown to an OD₆₀₀ of 0.8 before inducing expression by addition of 1 mM isopropyl β -D-1-thiogalactopyranoside. After 6 H of induction, cultures were spun at $5,000\times g$ for 30 Min. Cell pellets were frozen at -80 °C until used.

2.5. Protein purification

Cell pellets were resuspended in a wash buffer (100 mM Tris, 100 mM NaCl, 5 mM TCEP, pH 8.5) for lysis. A protease inhibitor was added, and the suspension was sonicated for 15 Min, on ice, at max amplitude for 10 Sec on and 10 Sec

off. Following sonication, lysed cells were spun at $25,000 \times g$ for 30 Min. For the histidine-containing proteins (S824 and DJB1), the lysates were incubated with NiNta resin for 15 Min at room temperature and then applied to a gravity flow column to allow unbound proteins to flow through. The column was washed with 10 column volumes of wash buffer to remove nonspecifically bound contaminants, and bundles were eluted with NiNta elution buffer (50 mM sodium phosphate, 10 mM Tris, 300 mM NaCl, 250 mM imidazole, pH 8).

The no-histidine bundles do not bind NiNta resins. Therefore, the sequences of S824-noHis and DJB1-noHis were modified to include a Strep-tag at their N-termini to facilitate affinity purification using the Strep-tag purification protocol [62].

A final purification step for all proteins was performed using reverse phase HPLC chromatography. Protein solutions were run through a Phenomenex (Torrance, CA, USA) C18 column at a flow rate of 5 mL/Min with an elution gradient starting near 100% aqueous (0.1% TFA) for 5 Min and ramping to 70% acetonitrile (0.1% TFA) in 50 Min. HPLC chromatograms for each purified protein are shown in Figure S7 in the Supporting Information. SDS-PAGE gels for the HPLC-purified proteins are shown in Figure S8 in the Supporting Information. Mass spectral data for bundles can be seen in Figures S9 and S10 in the Supporting Information.

2.6. Iron-sulfur cluster reconstitution

Lyophilized proteins were resolubilized in a deoxygenated buffer (100 mM Tris, 100 mM NaCl, pH 8.5) with an added reductant 10 mM dithiothreitol for 15 Min to reduce disulfide bonds. The protein stocks were diluted to concentrations of 200 μ M and then 10 molar equivalents of FeCl $_3$ (at a total concentration of 2 mM) were added and allowed to mix for 10 Min. This step was repeated, with additional 10 molar equivalents of FeCl $_3$ added and incubated for another 10 Min. Then the same two-step procedure was performed with Na $_2$ S, adding 10 molar equivalents on each step. The reaction mixture was allowed to incubate for 1 H at room temperature, and then passed through a GE Health Sciences (Marlborough, MA, USA) PD10 column to remove unbound (free) Fe $^{2+/3+}$ ions. The eluted solutions from PD10 were collected for further biophysical characterization.

2.7. Size exclusion chromatography

Size-exclusion chromatography (SEC) was performed anaerobically in a deoxygenated reconstitution buffer (100 mM Tris, 100 mM NaCl, pH 8.5). In all experiments, 200 μ L aliquots of protein at 140 μ M were injected into an anaerobically preequilibrated Superdex-75 column (GE Health Sciences, Marlborough, MA, USA), with a flow rate of 800 μ L/Min.

2.8. UV-visible redox titration

Redox titration experiments were performed in an anaerobic glove box. Protein samples were prepared at 70–140 μ M concentrations in deoxygenated buffers (100 mM Tris, 100 mM NaCl, pH 8.5). A Bio-Logic (Seyssinet-Pariset, France)



potentiostat (SP50) was used in a standard three-electrode configuration: a Pine Research gold honeycomb as a working electrode, an Ag/AgCl capillary tube as a reference electrode, and a platinum wire as a counterelectrode. UV-visible spectra were measured using a Cary 60 spectrophotometer, equipped with a fiber optic setup connected to the electrochemical cell inside the glove box. During the voltage scans, the samples were allowed to preequilibrate for 30 Min at each potential step before measuring the UV-visible spectrum.

The redox data were analyzed using the following form of a Nernst equation:

Absorbance =
$$\frac{A_1}{1 + \exp(n_1 F(E_1 - E)/RT)} + \frac{A_2}{1 + \exp(n_2 F(E_2 - E)/RT)}$$

where we consider two redox species in solution, with their redox potentials (E_i) , their population fractions (A_i) , and their numbers of redox electrons (n_i) . F is the Faraday constant, R is the universal gas constant, T is absolute temperature, and E is a set voltage during a titration scan. We found a good fit to our experimental titration curves (Fig. 3C) when assuming both $n_1 = n_2 = 1$.

2.9. Electron paramagnetic resonance spectroscopy

All electron paramagnetic resonance (EPR) samples were prepared anaerobically and were flash frozen in liquid nitrogen immediately after preparation. The final concentrations of DJB1-noHIS were in the range of 100–200 μ M in a reconstitution buffer (100 mM Tris, 100 mM NaCl, pH 8.5), containing 15–20% glycerol as a cryoprotectant. Freshly prepared sodium dithionite (2.5 mM) was added to reduce Fe₄S₄ clusters.

EPR experiments were performed on a Bruker (Billerica, MA, USA) EPR spectrometer (E580e) operating at X-band microwave frequency. A helium-flow cryostat, Oxford Instruments (Abingdon, Oxfordshire, UK) ESR900 and an Oxford Instruments temperature controller (ITC503) were used for cryogenic temperatures. Experiments were performed at temperature of 10 K with the following settings: microwave frequency, 9.49 GHz; microwave power, 200 μ W; modulation amplitude, 1–2 mT. The concentration of reduced [Fe₄S₄]¹⁺ clusters in each sample was determined by comparing the measured integrated signal intensity with the EPR standard of a known number of spins (a CuSO₄·5H₂O crystal of known weight in mineral oil). EPR simulations were performed using the EasySpin toolbox under MATLAB (Natick, MA, USA) (http://www.easyspin.org/).

2.10. Circular dichroism spectroscopy

Far UV circular dichroism (CD) experiments were performed on an Aviv (Lakewood, NJ, USA) CD spectrometer (model 420SF). Protein samples were diluted to 6–20 μ M in a buffer containing 33 mM Tris and 33 mM NaCl (pH 8.5). In addition,

the reductant, TCEP (2.5 mM), was added to the protein samples without reconstituted Fe/S to reduce all disulfide bonds. Spectra were measured anaerobically in 1 mm quartz cuvettes at 25 °C. The helical content of each sample was determined by decomposing the measured CD spectra using the published reference spectral components [63].

Thermal stability was examined by monitoring the intensity at 222 nm as a function of temperature. Temperature was increased in increments of 4 °C, and allowed to equilibrate for 5 Min between each measurement. The point where the observed 222-nm intensity dropped down to 50% of its maximum was defined at the melting temperature of the protein.

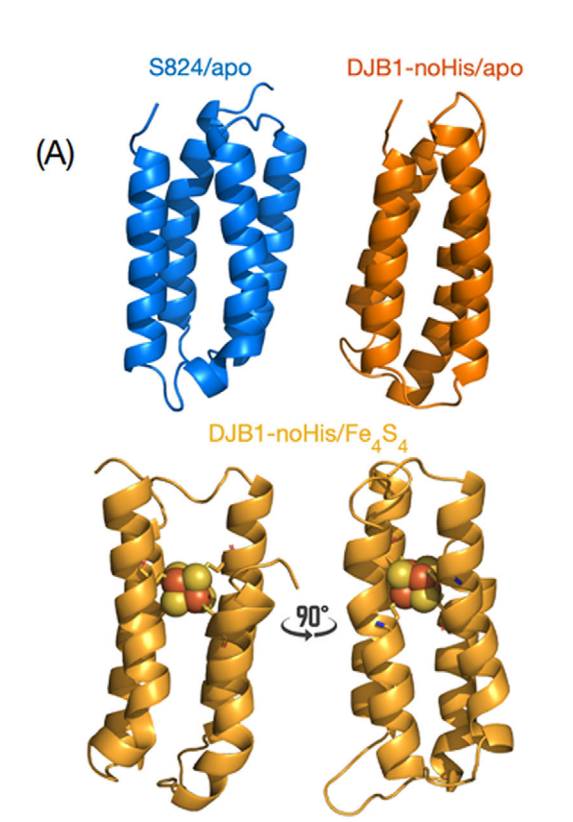
3. Results

3.1. Structure-based design

Protein S824 was chosen from a library of binary patterned four-helix bundles. The solution-NMR structure of S824 (PDB: 1p68) [35] shows a well-ordered, monomeric bundle; and biophysical characterization demonstrated high stability with a denaturation temperature near 100 °C [45]. The high stability of this protein suggested that it might tolerate the incorporation of substitutions that would be required to incorporate a buried Fe_4S_4 -binding site.

The solution-NMR structure of S824 was used as a starting template for designing a variant capable of binding a Fe₄S₄ cluster. The protein design software platform protCAD [57,58] was used to individually probe all core-facing positions for those capable of accommodating a Fe₄S₄ cluster. Initially, all side chains were removed from the structure, resulting in a polyalanine scaffold. Three rotameric degrees of freedom were sampled for cysteine ligated to a Fe₄S₄ cluster using ideal geometries for the cysteine-cluster coordination (Fig. 1A). This rapidly eliminated unfavorable cluster sites based on steric considerations. Position 64 was identified as the site with the fewest clashes with the S824 backbone, and the Fe₄S₄ coordination was completed by identifying core positions for three additional cysteine residues proximal to the remaining three irons of the Fe₄S₄ cluster. The remaining sequence of S824 was then remapped onto the scaffold, and three additional mutations were introduced to optimize core packing (see Methods) to produce the first design, DJB1. (Fig. 1B).

Subsequent modifications of DJB1 were designed to address experimental challenges. For example, initial characterization of DJB1, while demonstrating a successful Fe $_4$ S4 cluster incorporation via UV-visible absorption spectra (Figure S1A in the Supporting Information), was hampered by aggregation of the protein upon reconstitution with iron. We hypothesized that the aggregation was due to surface-exposed histidines on DJB1 inherited from S824, which could interact nonspecifically with Fe $^{2+/3+}$ present in the metal-reconstitution buffer [31]. Furthermore, when coordinated at the peripheral histidine sites, these Fe $^{2+/3+}$ ions could coordinate with histidine residues from neighboring DJB1 bundles, thereby causing bundle oligomerization (Figure S1B in the Supporting Information).



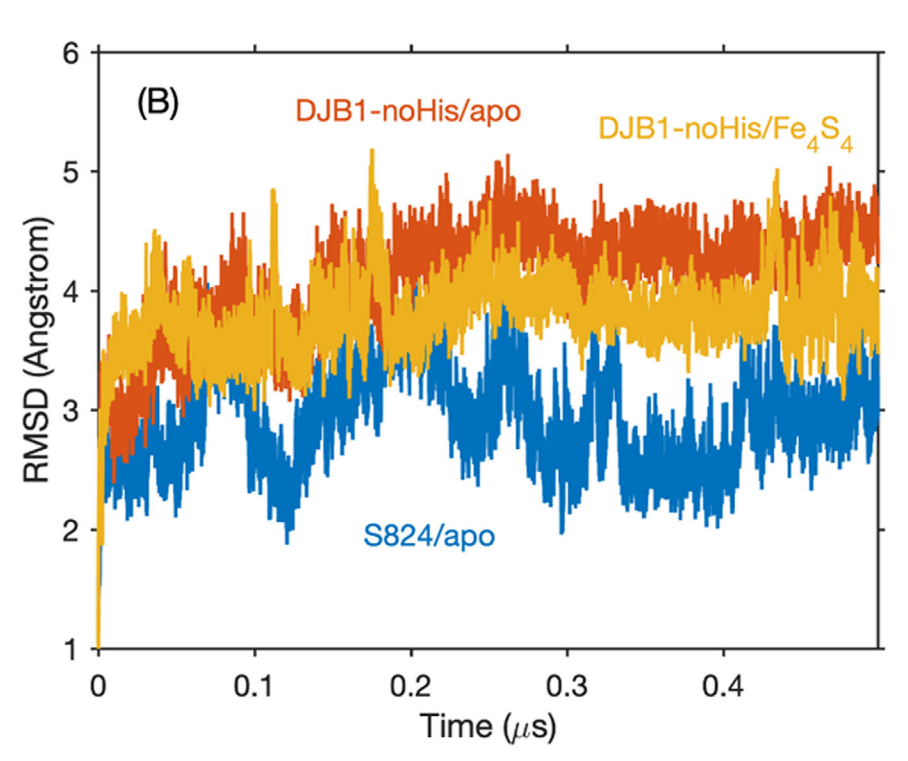


FIG. 2 MD simulations of DJB1-noHis, with and without Fe₄S₄, and the S824 parent control. (A) All modeled structures after $0.5~\mu s$ of MD optimization: (top left) The parent protein S824 starting from the NMR structure PDB:1p68 (blue); (top right) DJB1-noHis/apo designed for Fe₄S₄ coordination, without any metals bound (orange); and (bottom) two 90° rotations of DJB1-noHis with a Fe₄S₄ cluster coordinated (gold). (B) RMSD of backbone atom positions starting from the NMR-derived conformation of S824 (PDB: 1p68) over the course of the 0.5-μs MD run.

In order to alleviate these problems, we introduced surface mutations into the DJB1 design, replacing all histidine residues with either glutamine if in a helix, or serine if in a loop. This resulted in our final design variant DJB1-noHis (Fig. 1C). For control experiments, the same substitutions were introduced to the parent S824 sequence to produce S824-noHis.

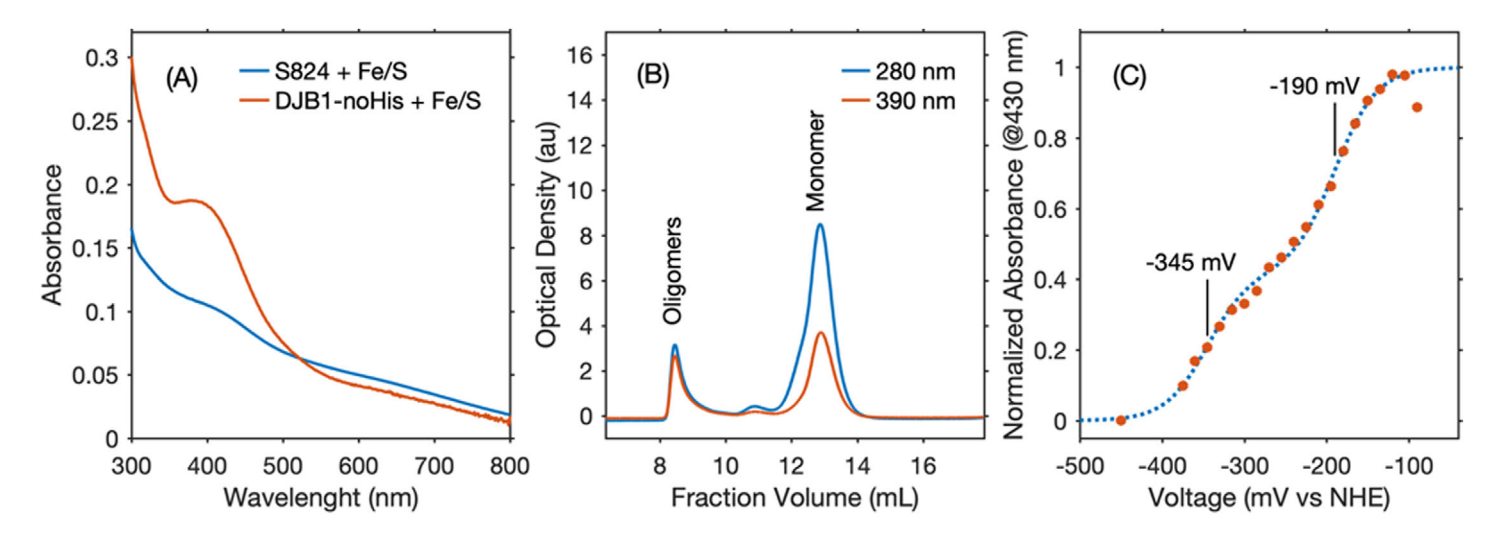
Conformational sampling of DJB1 and DJB1-noHis local side chain rotamer degrees of freedom was performed in protCAD. Next, extensive structural relaxation of the designs—with and without a reconstituted Fe₄S₄ cluster—was performed using MD simulations. All designs were simulated for 0.5 μ s in explicit water using the AMBER platform [54]. Both the metal bound (DJB1-noHis/Fe₄S₄) and free (DJB1-noHis/apo) models maintained their four-helix bundle structures over the entire simulation, and the structures were similar to the parent S824 (Fig. 2A). The average shifts in backbone atom positions in DJB1-noHis/Fe₄S₄ were less than 1 Å RMSD relative to S824, and even less than DJB1-noHis/apo (Fig. 2B).

Despite the global similarity of the designs to the parent fold, there were notable local changes in structure in DJB1-noHis/Fe $_4$ S $_4$, likely due to suboptimal metal coordination geometries in the initial structural models. The first and fourth helices shifted in opposite directions by about 3 Å each to relax strain associated with first-shell ligand coordination of the Fe $_4$ S $_4$ cluster (Figure S2 in the Supporting Information). Meanwhile, the second and third helices were pushed slightly away from each other by as much as 3 Å. Following this shift, the DJB1-noHis/Fe $_4$ S $_4$ remained constant, with an overall root mean square fluctuation of less than 0.2 Å Overall, these simulations suggest that while some rearrangements were required to accommodate metal coordination, the S824 scaffold likely would tolerate cluster incorporation the designed substitutions.

3.2. Expression and characterization

S824 and related designs were expressed in $E.\ coli$, purified, and then reconstituted with Fe/S as described in the Methods section. The reconstitution step was performed anaerobically in the presence of a 20-fold molar excess of Fe³⁺ and S²⁻. SEC was used to remove unbound ions and salts.

UV-visible absorption spectra of DJB1 and DJB1-noHis showed a well-defined peak at 430 nm (Fig. 3A and Figure S1A in the Supporting Information), which was absent in S824. This peak is characteristic of a thiolate-Fe $^{3+}$ charge-transfer transition [42] confirming incorporation of some form of Fe–S cluster. These Fe–S clusters could be either Fe $_4$ S $_4$ or Fe $_3$ S $_4$, or alternatively rubredoxin-like (single Fe $^{3+}$) centers, all of which would contribute to the absorption band at 430 nm with



Biophysical characterization of the Fe/S FIG. 3 reconstituted DJB1-noHis and S824 bundles: (A) UV-visible absorbance spectra of DJB1-noHis (red) and S824 (blue) in Tris pH 8 after Fe/S reconstitution. Absorbance intensities were normalized to a protein concentration of 140 μ M. The band at 430 nm in DJB1-noHis is characteristic of Fe-S clusters, including Fe₄S₄, Fe₃S₄, and rubredoxin-type, single Fe³⁺ centers. (B) Size exclusion chromatograms of DJB1-noHis in Tris pH 8, monitored at 280 nm (blue) and 390 nm (red), demonstrating the predominantly monomeric state of the Fe/S-reconstituted holo-DJB1-noHis. (C) UV-visible redox titration at 430 nm of holo-DJB1-noHis (red dots). The dashed blue line is a fit to the Nernst equation assuming two redox active species with potentials at -345 and -190 mV (vs NHE), and relative populations of 42% and 58%, respectively.

comparable extinction coefficients [64]. Given the broad range of extinction coefficients reported for Fe–S clusters (1,000– $10,000~1/\text{mol/L}\cdot\text{cm}$), it was difficult to estimate the yield of Fe–S cluster incorporation in DJB1 and DJB1-noHis, which could range from 10 to 100%.

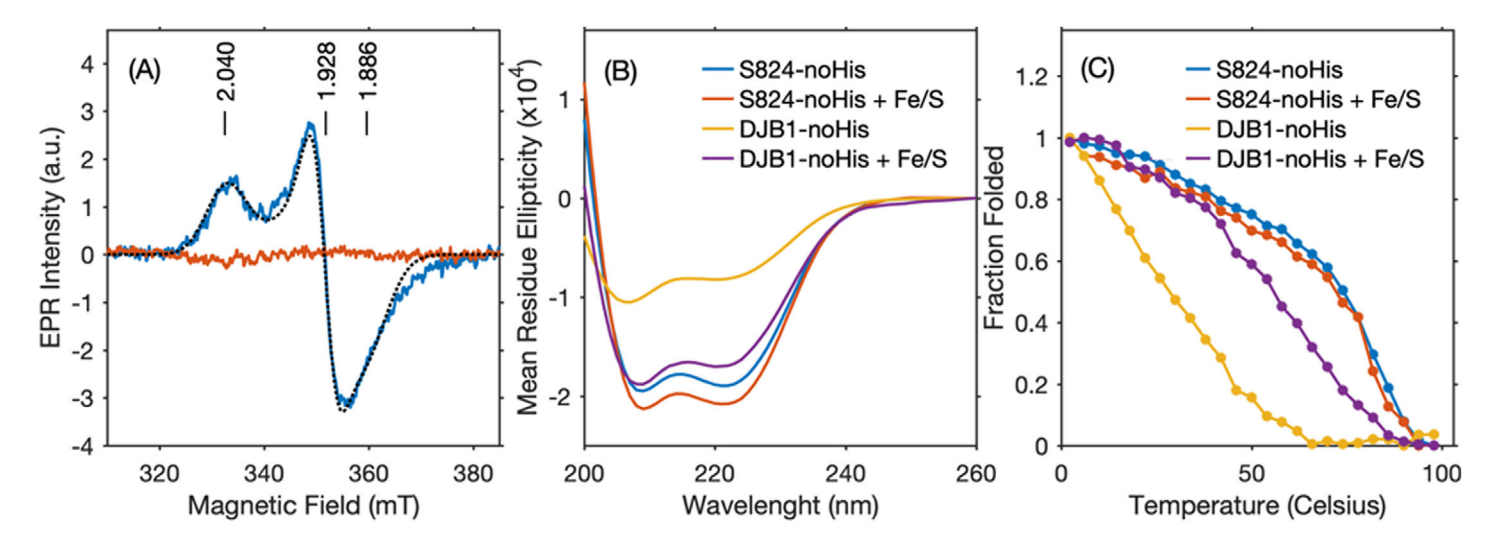
In the presence of Fe/S, SEC revealed complex oligomeric mixtures for the histidine-containing proteins, DJB1 and S824 (Figure S1B in the Supporting Information). We also observed that DJB1 and S824 completely precipitated from solution after a few days at room temperature in the presence of Fe/S. This Fe-induced oligomerization was presumably caused by 12 peripheral histidine residues present on the surfaces of S824 and DJB1 [31]. The Fe^{2+/3+} ions could coordinate with histidine ligands of two neighboring S824/DJB1 proteins, thereby nucleating aggregation. In addition to the oligomerization problem, these histidine ligands could potentially compete for Fe^{2+/3+}, thereby depleting its availability and interfering with formation of the desired Fe₄S₄ cluster.

As described earlier, histidines were removed in the DJB1-noHis and S824-noHis designs to minimize issues of aggregation and spectroscopic interference from nonspecific

metal coordination. In the presence of iron, DJB1-noHis eluted primarily as a monomer (estimated > 90%) in SEC profiles (Fig. 3B). The small oligomer peak still observed in the DJB1-noHis chromatogram may have resulted from interbundle Fe^{2+/3+} coordination through surface glutamates and aspartates [25,29]. Upon reconstitution with Fe/S, histidine-free designs were stable for days at room temperature, showing no sign of precipitation. Therefore, we focused further characterizations on the histidine-free variants, DJB1-noHis and S824-noHis.

Fe-S clusters can occupy a number of oxidation states over a wide range of potentials [44]. Electrochemical titrations were performed while monitoring absorption at 430 nm. DJB1-noHis exhibited a reversible, two-wave redox transition indicative of two redox-active Fe-S species (Fig. 3C). In comparison, no redox activity was observed for the control protein, S824 (Figure S3 in the Supporting Information). The titration curve of DJB1-noHis (Fig. 3C) was fit with the Nernst equation, which estimated two redox potentials at -345 and -190 mV (vs NHE), with relative populations of 42% and 58%, respectively, for the two redox-active Fe-S species. The potential at -345 mV is consistent with Fe₄S₄ clusters [42,44]. The identity of the −190 mV potential is less clear and could be from Fe₃S₄ clusters (e.g., degraded or partially reconstituted Fe₄S₄), or alternatively from a single Fe³⁺ in a rubredoxin-like coordination [42,44].

To further characterize the metalloproteins, we measured their EPR spectra. Each type of known Fe–S clusters has a unique EPR signature [65]. Fe₄S₄ clusters are expected to be paramagnetic in their reduced [Fe₄S₄]¹⁺ state, while Fe₃S₄ clusters and single-Fe centers are expected to be paramagnetic in their oxidized states, as [Fe₃S₄]¹⁺ and Fe³⁺, respectively. We performed EPR experiments on oxidized (resting state) and dithionite-reduced forms of reconstituted DJB1-noHis (Fig. 4A). In its oxidized state, reconstituted DJB1-noHis showed no EPR signals around g=2 (red trace in Fig. 4A). This suggested the bound clusters were not Fe₃S₄. In their typical three-cysteine coordination, the presence of Fe₃S₄ clusters would manifest as a distinct narrow peak at g=2.00–2.01 [66], which was



Structural characterization of the Fe/S FIG. 4 reconstituted DJB1-noHis: (A) EPR spectra of dithionite-reduced [Fe $_4$ S $_4$] $^{1+}$ in DJB1-noHis in Tris (pH 8), measured at 10 K with and without added sodium dithionite (blue and red traces, respectively). The black dash trace is a simulated EPR spectrum using a rhombic g-tensor = (2.040, 1.928, 1886), as marked with vertical lines. The estimated concentration of reduced [Fe₄S₄]¹⁺ is 60 μM, or 40% of total [DJB1-noHis]. (B) CD spectra in Tris (pH 8) at 25 °C, showing a recovery in the structural helicity of DJB1-noHis after its reconstitution with Fe/S. In contrast, for S824-noHis, the helicity stays high with or without Fe/S. (C) Thermal denaturation of DJB1-noHis and S824-noHis, monitored at 222 nm in the presence/absence of reconstituted Fe/S. The thermal stability of DJB1-noHis is partially restored after reconstituting with Fe/S.

not observed. However, the lack of observable EPR signal can also be interpreted as a "false negative." In principle, the Fe_3S_4 coordination in DJB1-noHis could be highly distorted in a way to produce a high-spin ground state configuration of Fe_3S_4 . Then this would make it unobservable by EPR [67,68].

The same oxidized DJB1-noHis sample, when measured at low magnetic fields, showed a narrow signal at g = 4.28with a weak shoulder at g = 5.2 (Figure S4 in the Supporting Information). This is a signature of single Fe³⁺ centers in a distorted tetrahedral ligand configuration (e.g., large zero field splitting (ZFS) greater than Zeeman interaction, D > $g\beta B_0$, and also large ZFS rhombicity, E/D \sim 1/3) [65] as has been reported for Fe³⁺ centers in several rubredoxins [66,69]. Although the data are consistent with Fe³⁺ centers in fourcysteine coordination in DJB1-noHis, this signal shape and the measured q-factors are not specific enough to make this assignment with certainty. Alternatively, this signal could originate from Fe³⁺ bound on the exterior of DJB1-noHis. This last interpretation is supported by the fact that a similar signal was also observed in the cysteine-free S824-noHis, although with slightly shifted *g*-factors.

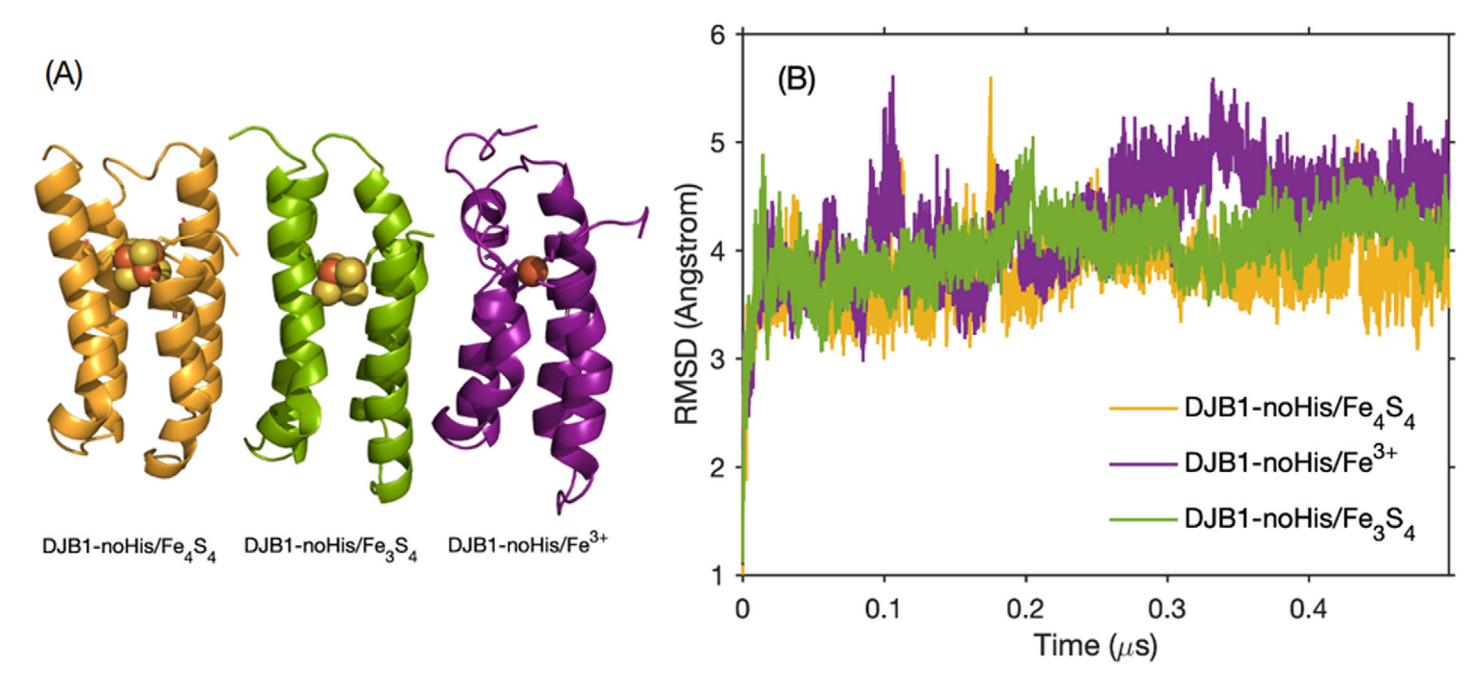
The reduced form of reconstituted DJB1-noHis (blue trace in Fig. 4A) revealed a strong EPR spectrum with a rhombic g-factor = (2.040, 1.928, 1886), consistent with the presence of reduced $[{\rm Fe_4S_4}]^{1+}$ clusters [66] From the signal intensity, we estimated that approximately 40% of the DJB1-noHis protein coordinates $[{\rm Fe_4S_4}]^{1+}$, consistent with the 42% estimated from the redox titration experiments (Fig. 3C), where the $-345~{\rm mV}$ transition was attributed to the $[{\rm Fe_4S_4}]^{2+}/^{1+}$ redox couple. To summarize, EPR positively identifies one of the redox-active species in DJB1-noHis as $[{\rm Fe_4S_4}]^{1+}$ clusters. The exact nature of the second redox-active species at $-190~{\rm mV}$ remains unclear, with both ${\rm Fe_3S_4}$ and single ${\rm Fe^{3+}}$ as possible candidates.

As noted above, S824 was selected as a starting scaffold because of its high stability that would allow this scaffold to tolerate a structurally destabilizing metal site. To assess stability of the designs, CD spectroscopy was used to probe α -helical content and its dependence on temperature (Figs. 4B and 4C). The control protein, S824-noHis, showed the highest helical content (estimated $\sim 60\%$ at 25 °C), and its CD spectrum did not change significantly upon addition of Fe/S. Moreover, the helicity and the stability of S824-noHis ($T_m \sim 74$ °C) were not altered by addition of metal. These observations were consistent with the lack of iron–sulfur coordination in the core of this control protein.

DJB1-noHis/apo at 25 °C had a lower helical content of 40% and a dramatically lower melting temperature of 28 °C. This destabilization presumably resulted from the reduced hydrophobicity and disrupted packing of the core-facing (cysteine) residues. Upon Fe/S reconstitution, DJB1-noHis/Fe₄S₄ showed an increased helicity of 52%, and an increased melting temperature of 56 °C (Figs. 4B and 4C). Apparently, the Fe–S cofactor binding in DJB1-noHis stabilized the design, partially compensating for the destabilizing effects from the cysteine core substitutions.

3.3. MD simulations of competing Fe-S states

As described above, spectroscopic characterization suggested that DJB1-noHis binds Fe_4S_4 with $\sim 40\%$ occupancy. The



MD simulations of DJB1-noHis with three types of Fe–S clusters incorporated. (A) Model structures optimized after MD runs for 0.5 μs: (left to right) DJB1-noHis/Fe₄S₄, DJB1-noHis/Fe₃S₄, and DJB1-noHis/Fe³⁺. (B) The RMSD of the backbone atom positions starting from the NMR-derived conformation of S824 (PDB: 1p68) over the course of the 0.5-μs MD run.

remaining 60% of the population was associated with a redox active species with a potential of -190 mV (Fig. 3C), which is in the range of Fe $_3$ S $_4$ clusters [42,44]. Fe $_3$ S $_4$ clusters could occur from incomplete reconstitution, or from degradation of a Fe $_4$ S $_4$ cluster [70,71]. Because of their structural similarity, Fe $_3$ S $_4$ could reasonably be expected to coordinate at a site designed for Fe $_4$ S $_4$. To further assess this possibility, we tested the stability of DJB1-noHis/Fe $_3$ S $_4$ in a long MD simulation, and, indeed, the Fe $_3$ S $_4$ bundle was as stable as the Fe $_4$ S $_4$ bundle (Fig. 5). Unfortunately, however, our EPR measurements could neither confirm nor rule out the presence of Fe $_3$ S $_4$.

An alternative candidate for the iron/sulfur species in 60% of DJB1-noHis could be single Fe^{3+} centers coordinated by cysteine. Although EPR measurements showed evidence of a Fe^{3+} -oxidized species (Figure S4 in the Supporting Information), it was not clear whether the Fe^{3+} coordination was mediated by core cysteines, or nonspecific coordination by glutamates or aspartates in the remaining oligomeric fraction of DJB1-noHis (Fig. 3B). Typical redox potentials for rubredoxin-like Fe^{3+} centers have been reported in the range from -50 to +50 mV (vs NHE) [42,44,72], which are slightly off from the observed -190 mV in our experiments. To model whether mononuclear metal coordination in DJB-noHis was feasible, MD simulations were performed to test the stability of a $(Cys)_4$ - Fe^{3+} site in DJB1-noHis. This simulation showed a greater loss of helicity

relative to either Fe_4S_4 or Fe_3S_4 . Four-cysteine coordination to a single Fe^{3+} required tighter interhelical distances, leading to unfavorable clashes.

3.4. Comparison to natural iron sulfur proteins

The iron–sulfur site designed into DJB differs from those found in nature in at least three ways: First, the cluster was designed into a fully α -helical topology. This has not been seen among natural iron–sulfur proteins. Second, the cluster was designed to be fully buried, whereas natural clusters are generally partially exposed to solvent. Third, our design included four cysteine side chains that were well separated in the primary sequence of the protein, which is dramatically different from the canonical Cys-X-X-Cys motif that is nearly universal among natural Fe–S proteins [60,73]. Despite these differences, this work confirms that such iron–sulfur designs can be redox active.

To assess whether a similar sequence motif has been found in nature, we used PSI-BLAST to search all nonredundant protein databases deposited in National Center for Biotechnology Information (NCBI) [74]. The closest similarities to DJB1-noHis were an uncharacterized protein (NCBI sequence id: XP_001023885) encoded in the ciliate Tetrahymena thermophila with a 33% sequence identity and a query coverage of 90%, and a HIV capsid protein (NCBI sequence id: AAF28639) with 33% sequence identity and 67% sequence coverage (Figure S5 in the Supporting Information). Neither of these proteins is known to coordinate metal ions. Interestingly, the segment of the capsid protein that aligns to the DJB1-noHis sequence is from position 47 to 77 (DJB1-noHis corresponding positions) which happens to include the two cysteines that coordinate the Fe-S cofactor. The capsid protein (e.g., 6MQP [75]) is fully helical with the aligned cysteines forming a disulfide bond. We did not discover any natural proteins that share structural

similarity or cofactor binding. Thus, the design of DJB1-noHis may reflect chemical and sequence space for metalloproteins that has not been explored by nature.

4. Discussion

The design process described in this study shows the potential to identify new scaffolds for binding multinuclear metal cofactors but also highlights the challenges associated with the optimization, characterization, and specificity of binding. DJB1-noHis bound the intended Fe₄S₄ cluster at \sim 40% occupancy. For the remaining 60% of the bundles, we do not have sufficient evidence to discriminate between Fe₃S₄ versus single Fe³⁺ centers, as the origin of the -190 mV potential. It possible both species contribute to the 60% of the population that is not occupied by Fe₄S₄. Future design iterations focusing on second shell mutations may produce a more specific binding site for Fe₄S₄.

The successes and challenges described in this study highlight the importance of considering both positive and negative designs. As discussed in some of the earliest papers on protein design [76,77], it is important not only to design toward a particular structure but also to design against competing alternatives. The design process for the DJB proteins illustrates several examples of positive and negative designs: In the firstgeneration design of DJB1, the computational method focused only on the core of the parent protein S824, where sampling of cysteine-cluster rotations and replacement of a few adjacent bulky residues with alanine, was all that was considered to design a Fe₄S₄ cluster into the bundle. Characterization of the purified protein by UV-vis spectroscopy showed a pronounced peak at 430, suggesting that the design had succeeded in producing an iron sulfur protein (Figure S1A in the Supporting Information).

However, further characterization showed that DJB1 formed large oligomers, not considered by the original design. This oligomerization presumably results from nonspecific Fe^{2+/3+} binding by histidines on the surface of two or more DJB1 molecules—a phenomenon that has also been observed for other proteins in binary-patterned libraries [31]. The abundance of these competing oligomers—and their subsequent precipitation—made it difficult to perform the detailed characterizations required to decipher which type of Fe–S was bound. To prevent precipitation, negative design was used to remove surface histidines that may favor metal-dependent oligomerization. This allowed characterization of design stabilities, metal incorporation, and redox potentials.

The ability of DJB1-noHis to potentially bind different forms of Fe–S is also observed in natural proteins, such as those involved in Fe–S cluster biosynthesis [78–81]. The Fe–S chaperone, IscU is proposed to initiate by recruiting Fe $^{3+}$ coordinated by cysteines in a loop region at the end of a helix [79], then assembling an intermediate Fe $_2$ S $_2$ cluster at the same site, and eventually converting it to an Fe $_4$ S $_4$ cluster [80,81]. The flexibility of IscU in binding the Fe–S cofactors of different

stoichiometries is associated with its cysteines being located on a flexible terminal loop. Similarly, the cysteines in DJB1 are located on different structural elements (different helices), enabling significant inter-ligand flexibility along the bundle axis, as seen in the MD simulation of DJB1-noHis (Figure S2 in the Supporting Information). This flexibility may be responsible for the observed promiscuity of Fe–S binding. With further design, this promiscuity may be exploited to control the cycling of redox active species for catalysis.

Unlike recent designs based on the ferredoxin fold [82] where iron–sulfur cluster assembly occurred *in vivo*, DJB1 required a separate chemical reconstitution step after purification. Perhaps this is because the biosynthetic machinery for inserting Fe_4S_4 into proteins evolved to recognize cysteines from local regions of sequence, which could be attached to Fe_4S_4 clusters at early stages in folding. In contrast, the cysteines from the four helices of DJB1 would likely come together only late in the folding of the bundle.

The burial of a charged Fe_4S_4 cofactor into the interior of a four-helix bundle would be expected to destabilize the hydrophobic core. While such destabilization was observed in our designs (Fig. 4), the high stability of the parental protein, S824, allowed the bundle to tolerate binding without unfolding. MD simulations indicate the core of DJB1-noHis could accommodate the charged cofactor by allowing partial solvation of the buried Fe_4S_4 cluster (Figure S6 in the Supporting Information). Partial solvent infiltration into the bundle core may explain the relatively low redox potential (-345~mV vs NHE) for Fe_4S_4 in DJB1-noHis.

As shown in CD studies, binding the Fe–S cluster stabilizes the structure of DJB1-noHis. DJB1-noHis/apo is less structured, likely due to lower core hydrophobicity relative to the parental protein, S824. MD simulations confirm DJB1-noHis/apo can form a four-helix bundle, but also explores alternative states. Formation of a structure that is preorganized for metal binding, but highly dynamic may be advantageous. Previous observations have shown that overdesign of stability can inhibit the cofactor binding and catalytic activity of artificial proteins [83,84] A combination of protein flexibility and an overall decrease in free energy accompanying cofactor binding is key to the design of cofactor-binding proteins.[85]

5. Conclusions

The process of producing DJB1 demonstrates how multinuclear metalloproteins may be derived from a combinatorial library of *de novo* sequences. The observed binding to DJB1 is nonspecific and seems to tolerate a range of different iron–sulfur clusters. Subsequent structure-guided design of the binding site to optimize metal coordination specificity and developing protocols to produce synthetic iron–sulfur metalloproteins *in vivo* are critical next steps in this project. The strategy described here set the stage for the future design of entire libraries of novel iron–sulfur proteins that can be subjected to screens and selections for novel redox-active catalysts.



6. Acknowledgements

The work was supported by a grant from the NASA Astrobiology Grant (Grant number 80NSSC18M0093) to VN. SP acknowledges funding from the NASA postdoctoral fellowship.

7. Conflict of Interest

The authors declare that they have no conflict of interest.

8. Data Availability

The data that support the findings of this study are available from the corresponding author upon reasonable request.

9. References

- [1] Liu, J., and Rost, B. (2001) Protein Sci. 10, 1970-1979.
- [2] Kamtekar, S., and Hecht, M. H. (1995) FASEB J. 9, 1013-1022.
- [3] Hill, R. B, Raleigh, D. P., Lombardi, A., and Degrado, W. F. (2000) Acc. Chem. Res. 33, 745–754.
- [4] Moelbert, S. (2004) Protein Sci. 13, 752-762.
- [5] Emberly, E. G., Wingreen, N. S., and Tang, C. (2002) Proc. Natl. Acad. Sci. 99, 11163–11168.
- [6] Kamtekar, S., Schiffer, J., Xiong, H., Babik, J., and Hecht, M. (1993) Science 262, 1680–1685.
- [7] Hecht, M. H., Das, A., Go, A., Bradley, L. H., and Wei, Y. (2004) Protein Sci. 13, 1711–1723.
- [8] Fisher, M. A., McKinley, K. L., Bradley, L. H., Viola, S. R., and Hecht, M. H. (2011) PLoS One 6, e15364.
- [9] Hoegler, K. J., and Hecht, M. H. (2016) Protein Sci. Publ. Protein Soc. 25, 1249–1259.
- [10] Digianantonio, K. M., and Hecht, M. H. (2016) Proc. Natl. Acad. Sci. 113, 2400–2405.
- [11] Digianantonio, K. M., Korolev, M., and Hecht, M. H. (2017) ACS Synth. Biol. 6, 694–700.
- [12] Donnelly, A. E., Murphy, G. S., Digianantonio, K. M., and Hecht, M. H. (2018) Nat. Chem. Biol. 14, 253–255.
- [13] Smith, B. A., Mularz, A. E., and Hecht, M. H. (2015) Protein Sci. Publ. Protein Soc. 24, 246–252.
- [14] Raanan, H., Poudel, S., Pike, D. H., Nanda, V., and Falkowski, P. G. (2020) Proc. Natl. Acad. Sci. 117, 7193–7199.
- [15] Li, Y., Drummond, D. A., Sawayama, A. M., Snow, C. D., Bloom, J. D., and Arnold, F. H. (2007) Nat. Biotechnol. 25, 1051–1056.
- [16] Bains, R. K., and Warren, J. J. (2016) Proc. Natl. Acad. Sci. 113, 248-250.
- [17] Watkins, D. W., Jenkins, J. M. X., Grayson, K. J., Wood, N., Steventon, J. W., Le Vay, K. K., Goodwin, M. I., Mullen, A. S., Bailey, H. J., Crump, M. P., Macmillan, F., Mulholland, A. J., Cameron, G., Sessions, R. B., Mann, S., and Anderson, J. L. R. (2017) Nat. Commun. 8, 358.
- [18] Lombardi, A., Summa, C. M., Geremia, S., Randaccio, L., Pavone, V., and Degrado, W. F. (2000) Proc. Natl. Acad. Sci. 97, 6298–6305.
- [19] Zastrow, M. L., Peacock, A. F. A., Stuckey, J. A., and Pecoraro, V. L. (2012) Nat. Chem. 4, 118–123.
- [20] Lombardi, A., Pirro, F., Maglio, O., Chino, M., and DeGrado, W. F. (2019) Acc. Chem. Res. 52, 1148–1159.
- [21] Plegaria, J. S., and Pecoraro, V.L. (2016) Methods Mol. Biol. Clifton NJ 1414, 187–196.
- [22] Chino, M., Leone, L., Maglio, O. & Lombardi, A. (2016) Methods Enzymol. 580, 471–499.
- [23] Zastrow, M. L., and Pecoraro, V. L. (2013) Coord. Chem. Rev. 257, 2565-2588.
- [24] Stenner, R., Steventon, J. W., Seddon, A., and Anderson, J. L. R (2020) Proc. Natl. Acad. Sci. 117, 1419–1428.
- [25] Farid, T. A., Kodali, G., Solomon, L. A., Lichtenstein, B. R., Sheehan, M. M., Fry, B. A., Bialas, C., Ennist, N. M., Siedlecki, J. A., Zhao, Z., Stetz, M. A.,

- Valentine, K. G., Anderson, J. L. R., Wand, A. J., Discher, B. M., Moser, C. C., and Dutton, P. L. (2013) Nat. Chem. Biol. 9, 826–833.
- [26] Ulas, G., Lemmin, T., Wu, Y., Gassner, G. T., and Degrado, W. F. (2016) Nat. Chem. 8, 354–359.
- [27] Moffet, D. A., Foley, J., and Hecht, M. H. (2003) Biophys. Chem. 105, 231-239.
- [28] Cook, S. A., and Borovik, A. S. (2015) Acc. Chem. Res. 48, 2407-2414.
- [29] Chino, M., Leone, L., Maglio, O., D'alonzo, D., Pirro, F., Pavone, V., Nastri, F., and Lombardi, A. (2017) Angew. Chem. Int. Ed. 56, 15580–15583.
- [30] Di Costanzo, L., Wade, H., Geremia, S., Randaccio, L., Pavone, V., Degrado, W. F., and Lombardi, A. (2001) J. Am. Chem. Soc. 123, 12749–12757.
- [31] Wang, M. S., Hoegler, K. J., and Hecht, M. H. (2019) Life 9.
- [32] Rojas, N. R., Kamtekar, S, Simons, C. T., McLean, J. E., Vogel, K. M., Spiro, T. G., Farid, R. S., and Hecht, M. H. (1997) Protein Sci. Publ. Protein Soc. 6, 2512–2524
- [33] Moffet, D. A., Certain, L. K., Smith, A. J., Kessel, A. J., Beckwith, K. A., and Hecht, M. H. (2000) J. Am. Chem. Soc. 122, 7612–7613.
- [34] Patel, S. C., Bradley, L. H., Jinadasa, S. P., and Hecht, M. H. (2009) Protein Sci. Publ. Protein Soc. 18, 1388–1400.
- [35] Wei, Y., Kim, S., Fela, D., Baum, J., and Hecht, M. H. (2003) Proc. Natl Acad. Sci. 100, 13270–13273.
- [36] Fontecave, M. (2006) Nat. Chem. Biol. 2, 171-174.
- [37] Poudel, S., Colman, D. R., Fixen, K. R., Ledbetter, R. N., Zheng, Y., Pence, N., Seefeldt, L. C., Peters, J. W., Harwood, C. S., and Boyd, E. S. (2018) J. Bacteriol. 200, e00757-17.
- [38] Poudel, S., Dunham, E. C., Lindsay, M. R., Amenabar, M. J., Fones, E. M., Colman, D. R., and Boyd, E. S. (2018) Front. Microbiol. 9.
- [39] Boyd, E. S., Amenabar, M. J., Poudel, S., and Templeton, A. S. (2020) Philos. Trans. R. Soc. Math. Phys. Eng. Sci. 378, 20190151.
- [40] Poudel, S., Tokmina-Lukaszewska, M., Colman, D. R., Refai, M., Schut, G. J., King, P. W., Maness, P. C., Adams, M. W.W., Peters, J. W., Bothner, B., and Boyd, E. S. (2016) Biochim. Biophys. Acta. 1860, 1910–1921.
- [41] Falkowski, P. G., and Raven, J. A. (2007) Aquatic Photosynthesis.
- [42] Beinert, H. (2000) J. Biol. Inorg. Chem. JBIC Publ. Soc. Biol. Inorg. Chem. 5, 2–15.
- [43] Matsubara, H., and Saeki, K. (1992) Adv. Inorg. Chem. 38, 223-280.
- [44] Stephens, P. J., Jollie, D. R., and Warshel, A. (1996) Chem. Rev. 96, 2491-2514.
- [45] Wei, Y. (2003) Protein Sci. Publ. Protein Soc. 12, 92-102.
- [46] Go, A., Kim, S., Baum, J., and Hecht, M. H. (2008) Protein Sci. Publ. Protein Soc. 17, 821–832.
- [47] Roy, A., Sommer, D. J., Schmitz, R. A., Brown, C. L., Gust, D., Astashkin, A., and Ghirlanda, G. (2014) J. Am. Chem. Soc. 136, 17343–17349.
- [48] Grzyb, J., Xu, F., Weiner, L., Reijerse, E. J., Lubitz, W., Nanda, V., and Noy, D. (2010) Biochim. Biophys. Acta 1797, 406–413.
- [49] Roy, A., Sarrou, I., Vaughn, M. D., Astashkin, A. V., and Ghirlanda, G. (2013) Biochemistry 52, 7586–7594.
- [50] Mejias, S. H., Bahrami-Dizicheh, Z., Liutkus, M., Sommer, D. J., Astashkin, A., Kodis, G., Ghirlanda, G., and Cortajarena, A. L. (2019) Chem. Commun. 55, 3319–3322.
- [51] Kim, J. D, Pike, D. H., Tyryshkin, A. M., Swapna, G. V. T., Raanan, H., Montelione, G. T., Nanda, V., and Falkowski, P. G. (2018) J. Am. Chem. Soc. 140. 11210–11213.
- [52] Mirts, E. N., Petrik, I. D., Hosseinzadeh, P., Nilges, M. J., and Lu, Y. I. (2018) Science 361, 1098–1101.
- [53] Nanda, V., Senn, S., Pike, D. H., Rodriguez-Granillo, A., Hansen, W. A., Khare, S. D., and Noy, D. (2016) Biochim. Biophys. Acta BBA - Bioenerg. 1857, 531–538
- [54] Ponder, J. W., and Case, D. A. (2003) Adv. Protein Chem. 66, 27-85.
- [55] Shapovalov, M. V., and Dunbrack, R. L. (2011) Struct. Lond. Engl. 1993 19, 844–858.
- [56] Schrödinger, L. L. C. The PyMOL Molecular Graphics System, Version 2.3. (2019).
- [57] Pike, D. H., Nanda, V. (2015) Biopolymers 104, 360-370.
- [58] Summa, C. M. (2002) Diss. Available ProQuest 1-479.
- [59] Maier, J. A., Martinez, C., Kasavajhala, K., Wickstrom, L., Hauser, K. E., and Simmerling, C. (2015) J. Chem. Theory Comput. 11, 3696–3713.

- [60] Kim, J. D, Rodriguez-Granillo, A., Case, D. A., Nanda, V., and Falkowski, P. G. (2012) PLoS Comput. Biol. 8,.
- [61] Humphrey, W., Dalke, A., Schulten, K. VMD: Visual molecular dynamics. J Mol Graphics 1996;14: 1:33–38.https://doi.org/10.1016/0263-7855(96)00018-5.
- [62] Strep-Tactin® protein purification resin | IBA Life sciences. Available at https://www.iba-lifesciences.com/isotope/2/2-1201-010-ShortProtocol_Strep-Tactin-Purification.pdf.
- [63] Wiedemann, C., Bellstedt, P., and Görlach, M. (2013) Bioinforma (Oxf. Engl). 29, 1750–1757.
- [64] Orme-Johnson, W. H. (1973) Annu. Rev. Biochem. 42, 159-204.
- [65] Hagen, W. R. (1992) Adv. Inorg. Chem. 38, 165-222.
- [66] Bertini, I., Ciurli, S., and Luchinat, C. (1995) In Iron-Sulfur Proteins Perovskites Springer, Berlin, pp. 1–53. https://doi.org/10.1007/3-540-59105-2_1.
- [67] Rothery, R. A., Bertero, M. G., Cammack, R., Palak, M., Blasco, F., Strynadka, N. C. J., Weiner, J. H. (2004) Biochemistry 43, 5324–5333.
- [68] Heinnickel, M., Agalarov, R., Svensen, N., Krebs, C., and Golbeck, J. H. (2006) Biochemistry 45, 6756–6764.
- [69] Peisach, J., Blumberg, W. E., Lode, E. T., and Coon, M. J. (1971) J. Biol. Chem. 246, 5877–5881.
- [70] Hosseinzadeh, P., and Lu, Y. I. (2016) Biochim. Biophys. Acta 1857, 557–581
- [71] Hoppe, A., Pandelia, M. -. E., Gärtner, W., and Lubitz, W. (2011) Biochim. Biophys. Acta 1807, 1414–1422.
- [72] Bill, E. (2013) In Yoshida, Y., Ed., ICAME 2011, Springer, Dordrecht, the Netherlands, pp. 287–295. https://doi.org/10.1007/978-94-007-4762-3_48.

- [73] Mulholland, S. E., Gibney, B. R., Rabanal, F., and Dutton, P. L. (1999) Biochemistry 38, 10442–10448.
- [74] Altschul, S. (1997) Nucleic. Acids. Res. 25, 3389-3402.
- [75] Smaga, S. S., Xu, C., Summers, B. J., Digianantonio, K. M., Perilla, J. R., and Xiong, Y. (2019) Struct. Lond. Engl. 27, 1234–1245.e5.
- [76] Hecht, M. H., Richardson, J. S., Richardson, D. C., and Ogden, R. C. (1990) Science 249, 884–891.
- [77] Regan, L., and Degrado, W. (1988) Science 241, 976-978.
- [78] Shimomura, Y., Wada, K., Fukuyama, K., and Takahashi, Y. (2008) J. Mol. Biol. 383, 133–143.
- [79] Wu, G., Mansy, S. S., Hemann, C., Hille, R., Surerus, K. K., and Cowan, J. (2002) J. Biol. Inorg. Chem. JBIC Publ. Soc. Biol. Inorg. Chem. 7, 526–532.
- [80] Agar, J. N., Krebs, C., Frazzon, J., Huynh, B. H., Dean, D. R., and Johnson, M. K. (2000) Biochemistry 39, 7856–7862.
- [81] Lin, C. W., Mccabe, J. W., Russell, D. H., and Barondeau, D. P. (2020) J. Am. Chem. Soc. 142, 6018–6029.
- [82] Mutter, A. C., Tyryshkin, A. M., Campbell, I. J., Poudel, S., Bennett, G. N., Silberg, J. J., Nanda, V., and Falkowski, P. G. (2019) Proc. Natl. Acad. Sci. 116, 14557–14562.
- [83] Schnatz, P. J., Brisendine, J. M., Laing, C. C., Everson, B. H., French, C. A., Molinaro, P. M., and Koder, R. L. (2020) Proc. Natl. Acad. Sci. 117, 5291–5297.
- [84] Cochran, F. V., Wu, S. P., Wang, W., Nanda, V., Saven, J. G., Therien, M. J., and Degrado, W. F. (2006) J. Am. Chem. Soc. 128, 663–663.
- [85] Polizzi, N. F., Wu, Y., Lemmin, T., Maxwell, A. M., Zhang, S. -. Q., Rawson, J., Beratan, D. N., Therien, M. J., and Degrado, W. F. (2017) Nat. Chem. 9, 1157–1164.